

ON MODULI OF RINGS AND QUADRILATERALS: ALGORITHMS AND EXPERIMENTS

HARRI HAKULA, ANTTI RASILA, AND MATTI VUORINEN

ABSTRACT. Moduli of rings and quadrilaterals are frequently applied in geometric function theory, see e.g. the Handbook by Kühnau. Yet their exact values are known only in a few special cases. Previously, the class of planar domains with polygonal boundary has been studied by many authors from the point of view of numerical computation. We present here a new hp -FEM algorithm for the computation of moduli of rings and quadrilaterals and compare its accuracy and performance with previously known methods such as the Schwarz-Christoffel Toolbox of Driscoll and Trefethen. We also demonstrate that the hp -FEM algorithm applies to the case of non-polygonal boundary and report results with concrete error bounds.

FILE: hrv.tex, 2010-03-20, printed: 2022-3-28, 4.35

1. INTRODUCTION

Plane domains with piecewise-smooth boundary curves occur in applications to electronics circuit design, airfoil modelling in computational fluid dynamics, computer vision and various other problems of engineering and science [23, 27, 28, 33, 37, 39]. We assume that the domain is bounded and that there are either one or two simple (and nonintersecting) boundary curves. The domain is then either simply or doubly connected. For the mathematical modelling of these domains it is usually convenient to map the domains conformally onto “canonical domains” as simple as possible: the unit disk $\mathbb{D} = \{z \in \mathbb{C} : |z| < 1\}$ or the annulus $\{z \in \mathbb{C} : r < |z| < 1\}$. Sometimes a rectangle is preferable to the unit disk as a canonical domain. The existence of these canonical conformal mappings is guaranteed by classical results of geometric function theory but the construction of this mapping in a concrete application case is usually impossible. Therefore one has to resort to numerical conformal mapping methods for which there exists an extensive literature [18, 28, 34, 37]. The Schwarz-Christoffel (SC) Toolbox of Driscoll [17], based on the software of Trefethen [41], is in wide use for numerical conformal mapping applications.

In the doubly connected case, one might be interested in only knowing the inner radius r of the canonical annulus. For instance this occurs if we wish to compute the electric resistance of a ring condenser. In this situation the conformal mapping itself is not needed if we are able to find the inner radius r by some other method. It is a classical fact that the inner radius r can be obtained in terms of the solution of the Dirichlet problem for the Laplace equation in the original domain with the boundary

1991 *Mathematics Subject Classification.* 65E05, 31A15, 30C85.

Key words and phrases. conformal capacity, conformal modulus, quadrilateral modulus, hp -FEM, numerical conformal mapping.

value 0 on one boundary component and the boundary value 1 on the other one. This fact is just one way of saying that the modulus of a ring domain is conformally invariant: for the canonical annulus $\{z \in \mathbb{C} : r < |z| < 1\}$ the modulus is equal to $\log(1/r)$. This idea reduces the problem of computing the number r to the problem of numerical approximation of the solutions of Laplace equation in ring domains. In the paper [9] this method was applied to several concrete examples of ring domains for which numerical results were reported, too. Again, it is also possible to use the Schwarz-Christoffel method for doubly connected domains [24].

We next consider the case of simply connected plane domains. For such a domain D and for a quadruple $\{z_1, z_2, z_3, z_4\}$ of its boundary points we call $(D; z_1, z_2, z_3, z_4)$ a quadrilateral if z_1, z_2, z_3, z_4 occur in this order when the boundary curve is traversed in the positive direction. The points $z_k, k = 1, \dots, 4$, are called the vertices and the part of the oriented boundary between two successive vertices such as z_1 and z_2 is called a boundary arc (z_1, z_2) . The modulus $M(D; z_1, z_2, z_3, z_4)$ of the quadrilateral $(D; z_1, z_2, z_3, z_4)$ is defined to be the unique $h > 0$ for which there exists a conformal mapping of D onto the rectangle with vertices $1 + ih, ih, 0, 1$ such that the points z_1, z_2, z_3, z_4 correspond to the vertices in this order. This conformal mapping is called the canonical conformal mapping associated with the quadrilateral. As in the case of doubly connected domains discussed above, it is well-known that the computation of the modulus h of the quadrilateral may be reduced to solving the Dirichlet-Neumann boundary value problem in the original domain D with the Dirichlet boundary values 1 on the boundary arc (z_1, z_2) and 0 on the arc (z_3, z_4) and Neumann boundary values 0 on the arcs (z_3, z_4) and (z_4, z_1) .

Conformal moduli of rings and quadrilaterals have independent theoretical interest because of their crucial role in the theory of quasiconformal mappings [29]. These quantities are closely related to certain physical constants, e.g. they play an important role in applications involving the measurement of resistance values of integrated circuit networks. But the problem of computing the moduli is also interesting in the wider engineering context. The reciprocal identities (4.1) and (6.3) can be used to generate test cases for curvilinear Lipschitz domains and thus should be standard tools in the FEM-software development community. Unfortunately these identities are missing from the introductory FEM textbooks. Even though our interest lies in the high-order methods, these test cases are equally valid for any numerical PDE methods and mesh adaptation in particular.

One specific application area of the algorithms presented here is the simulation of measurements for the 2D electrical impedance tomography (EIT) [25]. In EIT problems a number of electrodes are placed on the boundary of the domain and current patterns are considered between every pair of them. Indeed, computing the moduli can be considered as a very crude model for the so-called EIT background forward problem. In general, the meshes for the EIT forward problems can be adapted using the approaches outlined below. High level of accuracy is necessary for precise control of artificial noise in the simulations.

A general observation about the literature seems to be that reported numerical values of the moduli of concrete quadrilaterals (or ring domains) are hard to find in the literature. Perhaps the longest list of numerical results is given in [9] where

pointers to earlier literature may be found. The recent book [34] lists also many such numerical values. In our opinion a catalogue of these numerical values in the simplest cases would be desirable for instance for reference purposes. The book [37] and the paper [33, p. 127] list certain engineering formulas which have been applied in VLSI circuit design.

An outline of the structure of this paper now follows. First, in Section 2 we describe the methods used in this paper. In Section 3 we discuss in detail the various FEM methods used here, in particular the hp -method which was implemented and applied to generate some of the results reported below. Another method we use is the h -adaptive software package AFEM of K. Samuelsson, which implements an adaptive FEM method and which was previously used in [9]. In the present paper we use the AFEM method to compute the modulus of a quadrilateral whereas in [9] it was used merely for the computation of the moduli of ring domains. In Section 4 a test problem for quadrilaterals is described together with its analytic solution, following [22]. This analytic solution requires, however, an application of a numerical root finding program. Accordingly, this formula is analytic-numeric in its character. In Section 5 we check several methods against this analytic formula in a test involving a family of convex quadrilaterals. The methods discussed are the analytic formula from [22], the Schwarz-Christoffel Toolbox of [17, 18], the AFEM method of Samuelsson [9] and the present hp -method. On the basis of these experiments, an accuracy ranking of the methods is given in Section 5. In Section 6 the more general case of polygonal quadrilaterals is investigated, in particular L-shaped domains, and the results are compared to the literature. In Section 7 we discuss the computation of the modulus of a ring domain in a few special cases. For instance, for “the cross in square” ring domain considered previously in [9, Example 4] we now obtain much improved accuracy. In Section 8 we compute some examples with the hp -FEM which are difficult for other methods. In Section 9 our results and discoveries are summarized.

2. METHODS

The following problem is known as the *Dirichlét-Neumann problem*. Let D be a region in the complex plane whose boundary ∂D consists of a finite number of regular Jordan curves, so that at every point, except possibly at finitely many points, of the boundary a normal is defined. Let $\partial D = A \cup B$ where A, B both are unions of Jordan arcs. Let ψ_A, ψ_B be a real-valued continuous functions defined on A, B , respectively. Find a function u satisfying the following conditions:

- (1) u is continuous and differentiable in \overline{D} .
- (2) $u(t) = \psi_A(t)$, for all $t \in A$.
- (3) If $\partial/\partial n$ denotes differentiation in the direction of the exterior normal, then

$$\frac{\partial}{\partial n} u(t) = \psi_B(t), \quad \text{for all } t \in B.$$

2.1. Modulus of a quadrilateral and Dirichlét integrals. One can express the modulus of a quadrilateral $(D; z_1, z_2, z_3, z_4)$ in terms of the solution of the Dirichlét-Neumann problem as follows. Let $\gamma_j, j = 1, 2, 3, 4$ be the arcs of ∂D between (z_4, z_1) , (z_1, z_2) , (z_2, z_3) , (z_3, z_4) , respectively. If u is the (unique) harmonic solution of the

Dirichlét-Neumann problem with boundary values of u equal to 0 on γ_2 , equal to 1 on γ_4 and with $\partial u/\partial n = 0$ on $\gamma_1 \cup \gamma_3$, then by [1, p. 65/Thm 4.5]:

$$(2.2) \quad \mathbf{M}(D; z_1, z_2, z_3, z_4) = \int_D |\nabla u|^2 dm.$$

2.3. Modulus of a ring domain and Dirichlét integrals. Let E and F be two disjoint compact sets in the extended complex plane \mathbb{C}_∞ . Then one of the sets E, F is bounded and without loss of generality we may assume that it is E . If both E and F are connected and the set $R = \mathbb{C}_\infty \setminus (E \cup F)$ is connected, then R is called a *ring domain*. In this case R is a doubly connected plane domain. The *capacity* of R is defined by

$$\text{cap } R = \inf_u \int_R |\nabla u|^2 dm,$$

where the infimum is taken over all nonnegative, piecewise differentiable functions u with compact support in $R \cup E$ such that $u = 1$ on E . It is well-known that the harmonic function on R with boundary values 1 on E and 0 on F is the unique function that minimizes the above integral. In other words, the minimizer may be found by solving the Dirichlét problem for the Laplace equation in R with boundary values 1 on the bounded boundary component E and 0 on the other boundary component F . A ring domain R can be mapped conformally onto the annulus $\{z : e^{-M} < |z| < 1\}$, where $M = \mathbf{M}(R)$ is the *conformal modulus* of the ring domain R . The modulus and capacity of a ring domain are connected by the simple identity $\mathbf{M}(R) = 2\pi/\text{cap } R$. For more information on the modulus of a ring domain and its applications in complex analysis the reader is referred to [1, 23, 27, 29, 34].

In [34, Chapter 3] N. Papamichael and N. Stylianopoulos describe the so-called domain decomposition method for the computation of the modulus of a quadrilateral which is designed for the case of elongated quadrilaterals and applies e.g. to polygonal quadrilaterals that can be decomposed into simple pieces whose moduli can be estimated. As an example they consider a spiraling quadrilateral that can be decomposed into a “sum” of 13 trapezoids and report results that are expected to be correct up to 7 decimal places. Therefore, this method seems very attractive for the computation of the modulus of a special class of quadrilaterals. A key feature of the method is that it reduces the numerical difficulties caused by the crowding phenomenon for this special class of quadrilaterals.

2.4. Classification of methods for numerical computing. For the computation of the modulus of a quadrilateral or of a ring domain there are two natural approaches

- (1) methods based on the definition of the modulus and on the use of a conformal mapping onto a canonical rectangle or annulus,
- (2) methods that give only the modulus, not the canonical conformal map.

In some sense, methods of class (1) give a lot of extra information, namely the conformal mapping – all we want is a single real number. Methods of class (2) rely on solving the Dirichlét-Neumann boundary value problem or Dirichlét problem for the Laplace equation as described above.

In this paper we will mainly use methods of type (2) that make use of adaptive FEM methods for solving the Laplace equation.

2.5. Review of the literature on numerical conformal mapping. With the exception of a few special cases, both of the above methods lead to extensive numerical computation. For both classes of methods there are several options in the literature, see for instance the bibliography of [9]. Various aspects of the theory and practice of numerical conformal mapping are reviewed in the monographs [18, 28, 34, 37]. See also the authoritative surveys [20, 32, 42, 43].

Recently numerical conformal mappings have been studied from various points of view and in various applications by many authors, see e.g. [2, 8, 13, 14, 15, 26, 31, 35, 36].

3. p -, AND hp -FINITE ELEMENT METHOD

In the paper [9] the modulus of a ring domain was computed with the help of the software package AFEM of K. Samuelsson, based on an h -adaptive finite element method. It can be easily applied to compute the modulus of a quadrilateral.

In this section we describe the high-order p -, and hp -finite element methods and report the results of numerical computation of the moduli of a number of quadrilaterals. The paper of Babuška and Suri [7] gives an accessible overview of the method, for a more detailed exposition we refer to Schwab [38], and for those familiar with engineering approach the book by Szabo and Babuška [40] is recommended.

In the h -version or standard finite element method, the unknowns or degrees of freedom are associated with values at specified locations of the discretization of the computational domain, that is, the nodes of the mesh. In the p -method, the unknowns are coefficients of some polynomials that are associated with topological entities of the elements, nodes, sides, and interior. Thus, in addition to increasing accuracy through refining the mesh, we have an additional refinement parameter, the polynomial degree p .

Let us next define a p -type quadrilateral element. The construction of triangles is similar and can be found from the references given above.

3.1. Shape functions. Many different selections of shape functions are possible. We follow Szabo and Babuška [40] and present the so-called hierarchic shape functions.

Legendre polynomials of degree n can be defined using a recursion formula

$$(3.2) \quad (n+1)P_{n+1}(x) - (2n+1)xP_n(x) + nP_{n-1}(x) = 0, \quad P_0(x) = 1.$$

The derivatives can similarly be computed using a recursion

$$(3.3) \quad (1-x^2)P'_n(x) = -nP_n(x) + nP_{n-1}(x).$$

For our purposes the central polynomials are the integrated Legendre polynomials

$$(3.4) \quad \phi_n(\xi) = \sqrt{\frac{2n-1}{2}} \int_{-1}^{\xi} P_{n-1}(t) dt, \quad n = 2, 3, \dots$$

which can be rewritten as linear combinations of Legendre polynomials

$$(3.5) \quad \phi_n(\xi) = \frac{1}{\sqrt{2(2n-1)}} (P_n(\xi) - P_{n-2}(\xi)), \quad n = 2, 3, \dots$$

The normalizing coefficients are chosen so that

$$(3.6) \quad \int_{-1}^1 \frac{d\phi_i(\xi)}{d\xi} \frac{d\phi_j(\xi)}{d\xi} d\xi = \delta_{ij}, \quad i, j \geq 2.$$

We can now define the shape functions for a quadrilateral reference element. The shape functions are divided into three categories: nodal shape functions, side modes, and internal modes.

3.7. Nodal shape functions. There are four nodal shape functions.

$$\begin{aligned} N_1(\xi, \eta) &= \frac{1}{4}(1 - \xi)(1 - \eta), \\ N_2(\xi, \eta) &= \frac{1}{4}(1 + \xi)(1 - \eta), \\ N_3(\xi, \eta) &= \frac{1}{4}(1 + \xi)(1 + \eta), \\ N_4(\xi, \eta) &= \frac{1}{4}(1 - \xi)(1 + \eta). \end{aligned}$$

Taken alone, these shapes define the standard four-node quadrilateral finite element.

3.8. Side shape functions. There are $4(p-1)$ side modes associated with the sides of a quadrilateral ($p \geq 2$).

$$\begin{aligned} N_i^{(1)}(\xi, \eta) &= \frac{1}{2}(1 - \eta)\phi_i(\xi), \quad i = 2, \dots, p, \\ N_i^{(2)}(\xi, \eta) &= \frac{1}{2}(1 + \xi)\phi_i(\eta), \quad i = 2, \dots, p, \\ N_i^{(3)}(\xi, \eta) &= \frac{1}{2}(1 + \eta)\phi_i(\eta), \quad i = 2, \dots, p, \\ N_i^{(4)}(\xi, \eta) &= \frac{1}{2}(1 - \xi)\phi_i(\xi), \quad i = 2, \dots, p. \end{aligned}$$

3.9. Internal shape functions. For the internal modes we have two options. The so-called trunk space has $(p-2)(p-3)/2$ shapes

$$(3.10) \quad N_k^0(\xi, \eta) = \phi_i(\xi)\phi_j(\eta), \quad i, j \geq 2, \quad i + j = 4, 5, \dots, p,$$

whereas the full space has $(p-1)(p-1)$ shapes

$$(3.11) \quad N_k^0(\xi, \eta) = \phi_i(\xi)\phi_j(\eta), \quad i = 2, \dots, p, \quad j = 2, \dots, p,$$

where in both cases the index k depends on the chosen convention. In this paper we always use the full space. The internal shape functions are often referred to as bubble-functions.

3.12. Parity problem. The Legendre polynomials have the property $P_n(-x) = (-1)^n P_n(x)$. In 2D all internal edges of the mesh are shared by two different elements. We must ensure that each edge has the same global parameterization in both elements. This additional book-keeping is not necessary in the standard h -FEM.

3.13. Resource requirements. We have seen that the number of unknowns in a p -type quadrilateral is $(p+2)(p+3)/2$ or $4p+(p-1)^2$ if the internal modes are from trunk or full space, respectively. To compensate this, the number of elements is naturally taken to be as small as possible. Indeed, when the mesh is adapted in a suitable way, the dimension of the overall linear system can be significantly lower than in the corresponding h -method. However, the matrices tend to be denser in the p -method, so the space requirements in relation to the dimension of the linear system are greater for the p -method.

3.14. Proper grading of the meshes. For a certain class of problems it can be shown that if the mesh and the elemental degrees have been set optimally, we can obtain *exponential convergence*. A geometric mesh is such that each successive layer of elements changes in size with some *geometric scaling factor* α , toward some point of interest. In this case, the points of interest are always corner points.

The following theorem is due to Babuška and Guo [5]. Note that construction of appropriate spaces is technical. For rigorous treatment of the theory involved see Schwab [38], Babuška and Guo [6] and references therein.

3.15. Theorem. *Let $\Omega \subset \mathbb{R}^2$ be a polygon, v the FEM-solution, and let the weak solution u_0 be in a suitable countably normed space where the derivatives of arbitrarily high order are controlled. Then*

$$\inf_v \|u_0 - v\|_{H^1(\Omega)} \leq C \exp(-b\sqrt[3]{N}),$$

where C and b are independent of N , the number of degrees of freedom. Here v is computed on a proper geometric mesh, where the orders of individual elements depend on their originating layer, such that the highest layers have the smallest orders.

The result also holds for constant polynomial degree distribution.

Let us denote the number of the highest layer with ν , the *nesting level*. Using this notation we can refer to geometric meshes as (α, ν) -meshes.

In Figure 1 we show a geometric mesh template for a non-convex quadrilateral. Here we require that each node lies at the end point of an edge and that the meshlines follow the guidelines of the geometric meshes.

In Figure 2 a sequence of real p -type meshes is shown. The template mesh serves also as a pure p -type mesh where the approximation properties are changed only by varying the polynomial degree. In the middle and rightmost meshes the number of elements is the same because the nesting level is the same, only the scaling factor changes.

3.16. Generating geometric meshes. Here we consider generation of geometric meshes in polygonal domains. We use the following two-phase algorithm:

- (1) Generate a minimal mesh (triangulation) where the corners are isolated with a fixed number of triangles depending on the interior angle, θ so that the refinements can be carried out independently:
 - $\theta \leq \pi/2$: one triangle,
 - $\pi/2 < \theta \leq \pi$: two triangles, and
 - $\pi < \theta$: three triangles.

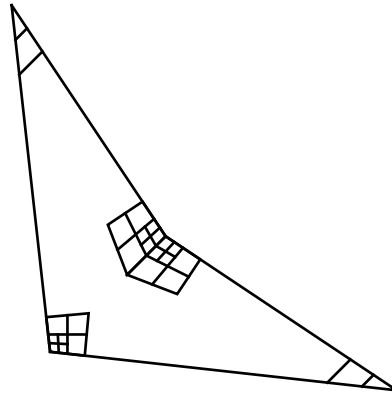


FIGURE 1. Geometric mesh for a general quadrilateral.

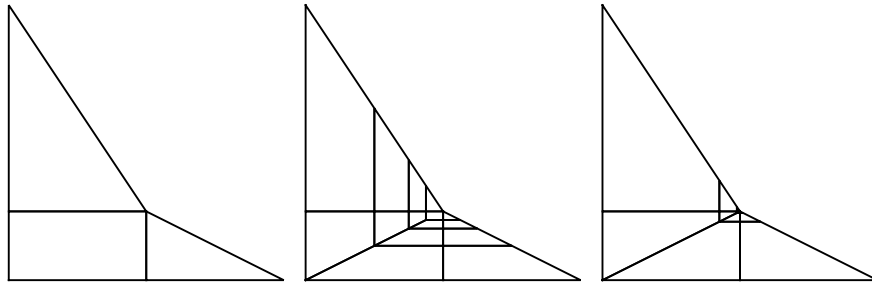


FIGURE 2. Graded meshes: Effect of the scaling factor. From left to right, template mesh, $(\alpha, \nu) = (1/2, 3)$, $(\alpha, \nu) = (1/6, 3)$.

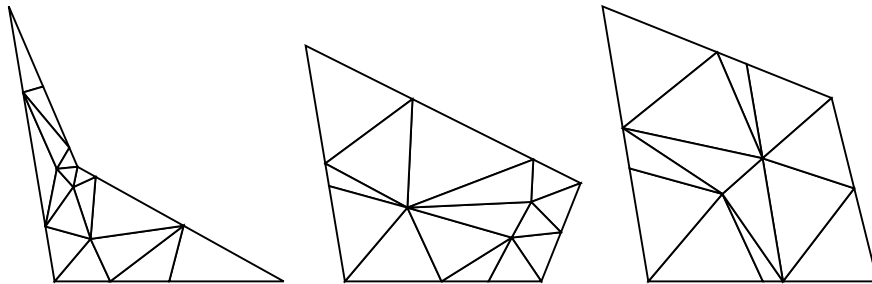


FIGURE 3. Three sample meshes used in numerical experiments below. Note the refinement of the mesh structure close to the corner points.

- (2) Every triangle attached to a corner is replaced by a refinement, where the edges incident to the corner are split as specified by the scaling factor α . This process is repeated recursively until the desired nesting level ν is reached. Note that the mesh may include quadrilaterals after refinement.

In Figure 2 we can also see our preferred element subdivisions: triangle to (quadrilateral, triangle)-pair, and quadrilateral to three quadrilaterals. These two rules are sufficient for our purposes since we always grade toward a corner point. Using this, we can derive a simple estimate for the number of degrees of freedom N .

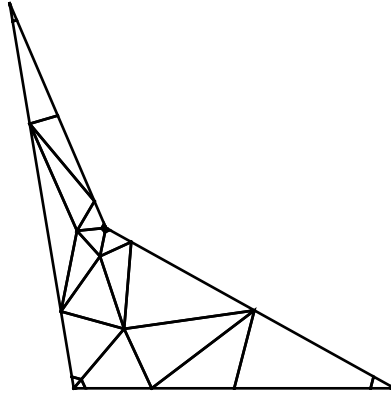


FIGURE 4. Final geometric or $(0.15, 12)$ -mesh. Due to small α only first two levels are visible.

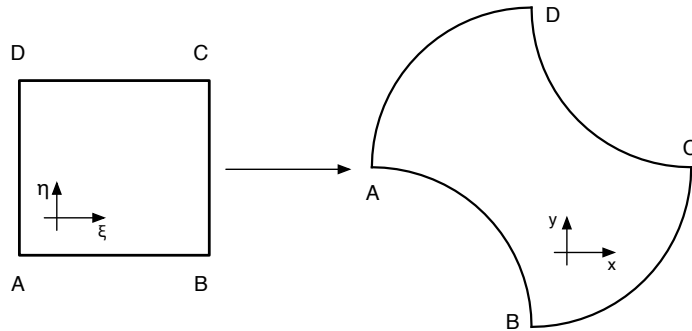


FIGURE 5. Curved boundary mapping.

Letting T denote the number of elements in the initial mesh, and C the number of corners in the domain (or those used in refining):

$$(3.17) \quad N \sim (T + 6C\nu)p^2,$$

where the constant 6 is the product of the maximal number of elements surrounding a corner, 3, and the maximal number of new elements per level, 2.

Finally, in Figure 3 three minimal meshes and in Figure 4 one final mesh are shown.

3.18. Domains with curved boundaries. Since we want to use as large elements as possible, it is important to represent curved boundary segments accurately. The linear blending function method of Gordon and Hall [21] is our choice for this purpose.

In the general case all sides of an element can be curved as in Figure 5. We assume that every side is parameterized:

$$(3.19) \quad x = x_i(t), \quad y = y_i(t), \quad -1 \leq t \leq 1, \quad i = 1, \dots, \text{number of sides}$$

Using capital letters as coordinates of the corner points, (X_i, Y_i) , we can write the mapping for the global x -coordinates of a quadrilateral as

$$(3.20) \quad \begin{aligned} x &= \frac{1}{2}(1 - \eta)x_1(\xi) + \frac{1}{2}(1 + \xi)x_2(\eta) + \frac{1}{2}(1 + \eta)x_3(\xi) + \frac{1}{2}(1 - \xi)x_4(\eta) \\ &- \frac{1}{4}(1 - \xi)(1 - \eta)X_1 - \frac{1}{4}(1 + \xi)(1 + \eta)X_2 - \frac{1}{4}(1 + \xi)(1 + \eta)X_3 \\ &- \frac{1}{4}(1 - \xi)(1 + \eta)X_4, \end{aligned}$$

and symmetrically for the y -coordinate. Note, that if the side parameterizations represent straight edges, the mapping simplifies to the standard bilinear mapping of quadrilaterals.

In the following we always use exact representation of the geometry which implies that in the ensuing mesh grading process no approximation of geometry is necessary. Here the mesh generation of the curved domains is template-based, thus the changes in curvature are not automatically dealt with. For a highly accessible review of the p -method mesh generation issues we refer to [30].

4. CONVEX QUADRILATERAL

In this section our goal is to introduce a test problem, whose solution is determined by a transcendental equation. This equation can be numerically solved to the desired accuracy and we will use this to check the validity of the numerical methods we use as well as to obtain an experimental estimate for their accuracy. The test problems we consider are convex polygonal quadrilaterals. The simplest such quadrilateral consists of the four vertices and the line segments joining the vertices. Let $z_1, z_2, z_3, z_4 \in \mathbb{C}$ be distinct points and suppose that the polygonal line that results from connecting these points by segments in the order z_1, z_2, z_3, z_4, z_1 forms the positively oriented boundary of a domain Q . For simplicity, we denote by $\text{QM}(z_1, z_2, z_3, z_4)$ the modulus $\text{M}(Q; z_1, z_2, z_3, z_4)$. Then the modulus is a conformal invariant in the following sense: If $f: Q \rightarrow fQ$ is a conformal mapping onto a Jordan domain fQ , then f has a homeomorphic extension to the closure \bar{Q} (also denoted by f) and

$$\text{M}(Q; z_1, z_2, z_3, z_4) = \text{M}(fQ; f(z_1), f(z_2), f(z_3), f(z_4)).$$

It is clear by geometry that the following reciprocal identity holds:

$$(4.1) \quad \text{M}(Q; z_1, z_2, z_3, z_4)\text{M}(Q; z_2, z_3, z_4, z_1) = 1.$$

If $h: \mathbb{C} \rightarrow \mathbb{C}$ is a translation, rotation, or stretching, then the piecewise linear nature of the boundary is preserved and we can write the conformal invariance simply as

$$\text{QM}(z_1, z_2, z_3, z_4) = \text{QM}(f(z_1), f(z_2), f(z_3), f(z_4)).$$

There are two particular cases, where we can immediately give $\text{QM}(z_1, z_2, z_3, z_4)$. The first case occurs, when all the sides are of equal length (i.e. the quadrilateral is a rhombus) and in this case the modulus is 1, see [22]. In the second case $(Q; z_1, z_2, z_3, z_4)$ is the rectangle $(Q; 1+ih, ih, 0, 1)$, $h > 0$, and $\text{QM}(1+ih, ih, 0, 1) = h$.

4.2. Basic identity. In [22, 2.11] some identities satisfied by the function $\text{QM}(a, b, 0, 1)$ were pointed out. We will need here the following one, which is the basic reciprocal identity (4.1) rewritten for the expression QM :

$$(4.3) \quad \text{QM}(a, b, 0, 1) \cdot \text{QM}((b-1)/(a-1), 1/(1-a), 0, 1) = 1.$$

We shall consider here the following particular cases of this reciprocal identity: (a) parallelogram, (b) trapezoid with angles $(\pi/4, 3\pi/4, \pi/2, \pi/2)$, and (c) a convex polygonal quadrilateral. Note that for the cases (a) and (b) the formula is less complex than for the general case (c).

4.4. The hypergeometric function and complete elliptic integrals. Given complex numbers a, b , and c with $c \neq 0, -1, -2, \dots$, the *Gaussian hypergeometric function* is the analytic continuation to the slit plane $\mathbb{C} \setminus [1, \infty)$ of the series

$$(4.5) \quad F(a, b; c; z) = {}_2F_1(a, b; c; z) = \sum_{n=0}^{\infty} \frac{(a, n)(b, n)}{(c, n)} \frac{z^n}{n!}, \quad |z| < 1.$$

Here $(a, 0) = 1$ for $a \neq 0$, and (a, n) is the *shifted factorial function* or the *Appell symbol*

$$(a, n) = a(a+1)(a+2) \cdots (a+n-1)$$

for $n \in \mathbb{N} \setminus \{0\}$, where $\mathbb{N} = \{0, 1, 2, \dots\}$ and the *elliptic integrals* $\mathcal{K}(r), \mathcal{K}'(r)$ are defined by

$$\mathcal{K}(r) = \frac{\pi}{2} F(1/2, 1/2; 1; r^2), \quad \mathcal{K}'(r) = \mathcal{K}(r'), \quad \text{and } r' = \sqrt{1-r^2}.$$

Some basic properties of these functions can be found in [4].

4.6. Parallelogram. For $t \in (0, \pi)$ and $h > 0$ let

$$g(t, h) \equiv \text{QM}(1 + he^{it}, he^{it}, 0, 1).$$

An analytic expression for this function has been given in [3, 2.3]:

$$(4.7) \quad g(t, h) = \mathcal{K}'(r_{t/\pi}) / \mathcal{K}(r_{t/\pi}),$$

where

$$(4.8) \quad r_a = \mu_a^{-1} \left(\frac{\pi h}{2 \sin(\pi a)} \right), \quad \text{for } 0 < a \leq 1/2,$$

and the decreasing homeomorphism $\mu_a: (0, 1) \rightarrow (0, \infty)$ is defined by

$$(4.9) \quad \mu_a(r) \equiv \frac{\pi}{2 \sin(\pi a)} \frac{F(a, 1-a; 1; 1-r^2)}{F(a, 1-a; 1; r^2)}.$$

4.10. Theorem. [22] *Let $0 < a, b < 1$, $\max\{a+b, 1\} \leq c \leq 1 + \min\{a, b\}$, and let Q be the quadrilateral in the upper half plane $\mathbb{H} = \{z \in \mathbb{C} : \text{Im } z > 0\}$ with vertices $0, 1, A$ and B , the interior angles at which are, respectively, $b\pi, (c-b)\pi, (1-a)\pi$ and $(1+a-c)\pi$. Then the conformal modulus of Q is given by*

$$(4.11) \quad \text{QM}(A, B, 0, 1) \equiv \mathbf{M}(Q) = \mathcal{K}(r') / \mathcal{K}(r),$$

where $r \in (0, 1)$ satisfies the equation

$$(4.12) \quad A - 1 = \frac{Lr'^{2(c-a-b)}F(c-a, c-b; c+1-a-b; r'^2)}{F(a, b; c; r^2)},$$

say, and

$$L = \frac{B(c-b, 1-a)}{B(b, c-b)}e^{(b+1-c)i\pi}.$$

For a fixed complex number b with $\text{Im}(b) > 0$ define the following function $g(x, y) = \text{QM}(x + i \cdot y, b, 0, 1)$ for $x \in \mathbb{R}$, $y > 0$. This is well-defined only if the polygonal domain with vertices $x + i \cdot y$, b , 0 , 1 is positively oriented. This holds e.g. if $\text{Re}(b) < 0$ and $x > 0$. It is a natural question to study the level sets of the function g . This function tells us how the modulus of a polygonal quadrilateral changes when three vertices are kept fixed and the fourth one is moving. For instance, it was shown in [19] that the function decreases when we move the fourth vertex into certain directions.

4.13. Trapezoid (Burnside [12]). In [9, pp. 237-239] so called square frame, the domain between two concentric squares with parallel sides, was considered. Such a domain can be split into 8 similar quadrilaterals, and we shall study here one such quadrilateral with vertices $1 + hi$, $(h-1)i$, 0 , and 1 , $h > 1$. When $h > 1$ we have by [10, pp. 103-104], [12]

$$(4.14) \quad \mathbf{M}(Q; 1 + hi, (h-1)i, 0, 1) \equiv M(h) \equiv \mathcal{K}(r)/\mathcal{K}(r')$$

where

$$r = \left(\frac{t_1 - t_2}{t_1 + t_2} \right)^2, \quad t_1 = \mu_{1/2}^{-1} \left(\frac{\pi}{2c} \right), \quad t_2 = \mu_{1/2}^{-1} \left(\frac{\pi c}{2} \right), \quad c = 2h - 1.$$

Therefore, the quadrilateral can be conformally mapped onto the rectangle $1 + iM(h)$, $iM(h)$, 0 , 1 , with the vertices corresponding to each other. It is clear that $h - 1 \leq M(h) \leq h$. The formula (4.12) has the following approximative version

$$M(h) = h + c + O(e^{-\pi h}), \quad c = -1/2 - \log 2/\pi \approx -0.720636,$$

given in [33]. As far as we know there is neither an explicit nor asymptotic formula for the case when the angle $\pi/4$ of the trapezoid is replaced by an angle equal to $\alpha \in (0, \pi/2)$.

4.15. Numerical computation of elliptic integrals. The computation of the elliptic integrals is efficiently carried out by classical methods available in most programming environments. Numerical estimates for $\mathcal{K}(r)$, and hence for $\mu_{1/2}(r)$, are obtained very efficiently by the following recursive method. For $r \in (0, 1)$ let

$$\begin{cases} a_0 = 1, & b_0 = r' \in (0, 1), \\ a_{n+1} = (a_n + b_n)/2, & b_{n+1} = \sqrt{a_n b_n}, \end{cases}$$

Then the sequences (a_n) and (b_n) have the common limit $\pi/(2\mathcal{K}(r))$, and, for each $y \in (0, \infty)$ we can approximate $\mu_{1/2}^{-1}(y)$ numerically by the Newton-Raphson iteration. For details. see e.g. [4, 3.22, 5.32] and [22, 2.11].

5. VALIDATION OF ALGORITHMS: CONVEX QUADRILATERALS

Validation of the algorithms for the modulus of a quadrilateral will be discussed in two main cases: convex quadrilaterals and the case of a general polygonal quadrilateral. In this section the case of a convex quadrilateral will be discussed for the following three algorithms: (a) the SC Toolbox in MATLAB written by Driscoll [17], (b) the AFEM software due to Samuelsson [9], (c) the hp -method of the present paper implemented in the Mathematica language using the double precision. The reference computation is carried out by the algorithm of [22], implemented in [22] in the Mathematica language (the algorithm $\text{QM}[A,B]$ implementing the formula in Theorem 4.10). This implementation makes use of multiple precision arithmetic for root finding of a transcendental equation involving the hypergeometric function. All the SC Toolbox tests in this paper were carried out with the settings `precision = 1e-14`.

5.1. Setup of the validation test. All our tests were carried out in the same fashion using the reciprocal identity (4.3) and considering a quadrilateral with the vertices $a, b, 0, 1$ with $\text{Im } a > 0$, $\text{Im } b > 0$, and the line segments joining the vertices as the boundary arcs. The vertices $b, 0, 1$ were kept fixed and the vertex a varied over a rectangular region in the complex plane. The numerical value $b = -0.2 + i \cdot 1.2$ was used and the lower left (upper right) corner of the rectangular region was $0.5 + i \cdot 0.2$ ($1.5 + i \cdot 1.2$). Examples of such quadrilaterals, along with some minimal meshes used in the computation, are illustrated in Figure 3. The test functional, based on the reciprocal identity (4.3), is

$$(5.2) \quad \text{test}(a, b) = \left| \text{QM}(a, b, 0, 1) \text{QM}\left(\frac{b-1}{a-1}, 1, 1/(1-a), 0, 1\right) - 1 \right|$$

which vanishes identically. The values of this test functional are reported in Table 1 for the fixed value $b = -0.2 + i \cdot 1.2$ when a runs through the aforementioned rectangular region. A table of values of $\text{QM}(m + in, i, 0, 1)$, $m, n = 1, \dots, 5$ is given in [22, Table1].

TABLE 1. Tests related to the convex quadrilateral, with (0.15, 18)-meshes used in the hp -method.

Method	Error range	
AFEM	$1.15 \cdot 10^{-11}$	$1.41 \cdot 10^{-8}$
SC Toolbox	$1.11 \cdot 10^{-16}$	$1.55 \cdot 10^{-14}$
hp -method ($p = 12$)	$6.51 \cdot 10^{-14}$	$7.84 \cdot 10^{-9}$
hp -method ($p = 15$)	$2.22 \cdot 10^{-16}$	$1.42 \cdot 10^{-10}$
hp -method ($p = 18$)	$1.11 \cdot 10^{-16}$	$3.90 \cdot 10^{-12}$

5.3. The reference computation. We used the Mathematica script of [22] for solving the equation in Theorem 4.10 for the computation of $\text{QM}(a, b, 0, 1)$ in order to carry out the test. The conclusion was that the amplitude of the error was roughly 10^{-17} i.e. there was practically no error. Note that the quadrilateral here is not always convex. On the basis of numerical experiments, it seems that the reference method

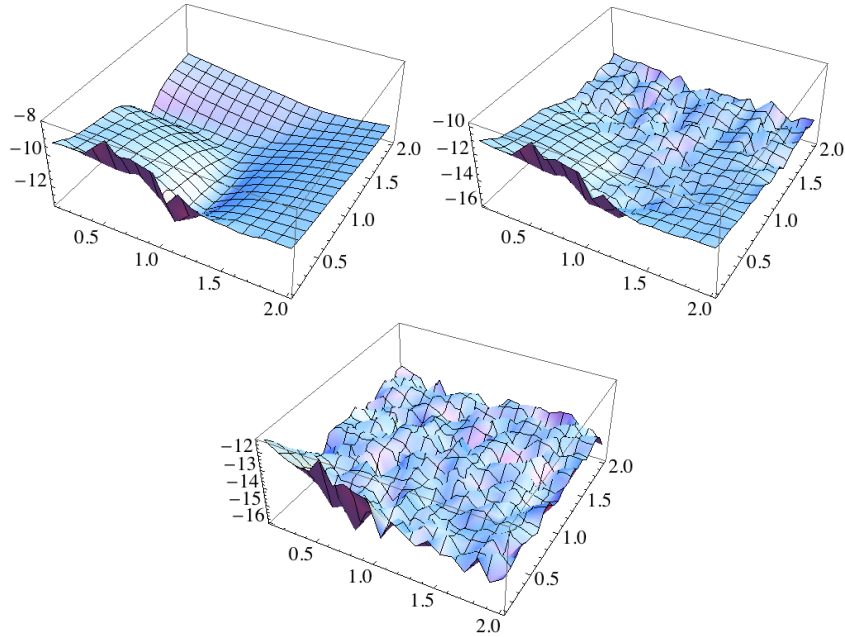


FIGURE 6. Logarithm (with base 10) of errors over the domain $[0.1, 2] \times [0.1, 2]$, corresponding to values of $p = 12, 15, 18$ starting from above. The error estimate is obtained by using the identity (4.3).

of [22] does also work in non-convex cases, but this has not been rigorously proved. These results were then compared to numerical values obtained by using AFEM, SC Toolbox and the hp -method. The results are summarized in Table 1.

6. VALIDATION: POLYGONAL QUADRILATERALS

In this section we will consider the validation of the algorithms for the modulus of a quadrilateral in the case of polygonal domains with $q > 4$ vertices. In the case considered in the previous section there was a reference computational method, providing the reference value for the moduli. There is no similar formula available for the general polygonal case.

6.1. Setup of the validation test. All our tests were carried out in the same fashion as in the previous section, using the reciprocal identity (4.3). We selected a quadruple of points $\{z_1, z_2, z_3, z_4\}$, which is a subset of the set of vertices defining the polygon D , and assume that these are positively oriented. Thus $(D; z_1, z_2, z_3, z_4)$ is a quadrilateral to which the reciprocal identity (4.3) applies.

6.2. The notation $\text{cmodu}(w, k_1, k_2)$ and $\text{modu}(w, k_1, k_2)$. Suppose that w is a vector of p complex numbers such that the points w_1, \dots, w_q , $q \geq 5$, are the vertices of a polygon D and that they define a positive orientation of the boundary. Choose indices $k_1, k_2 \in \{1, \dots, p-1\}$ with $k_1 < k_2$ and set $z_1 = w_{k_1}$, $z_2 = w_{k_1+1}$, $z_3 = w_{k_2}$, $z_4 = w_{k_2+1}$. Then we define

$$\text{cmodu}(w, k_1, k_2) = \mathbf{M}(D; z_1, z_2, z_3, z_4), \quad \text{modu}(w, k_1, k_2) = \mathbf{M}(D; z_2, z_3, z_4, z_1).$$

By the reciprocal relation (4.1) we have

$$(6.3) \quad \text{cmodu}(w, k_1, k_2) \cdot \text{modu}(w, k_1, k_2) = 1.$$

6.4. L-shaped region. The L-shaped region:

$$L(a, b, c, d) = L_1 \cup L_2, \quad L_1 = \{z \in \mathbb{C} : 0 < \text{Re}(z) < a, 0 < \text{Im}(z) < b\},$$

$$L_2 = \{z \in \mathbb{C} : 0 < \text{Re}(z) < d, 0 < \text{Im}(z) < c\}, \quad 0 < d < a, \quad 0 < b < c,$$

is a standard domain considered by several authors for various computational tasks. In the context of computation of the moduli it was investigated by Gaier [20] and we will compare our results to his results. In the test cases all the vertices had integer coordinates in the range $[1, 4]$. Since we consider an integer coordinate domain, simple quadrilateral grid has the desired properties of the minimal mesh. An example of such a mesh is shown in Figure 9. The results are summarized in Table 2, and the potential functions are illustrated by Figure 7.

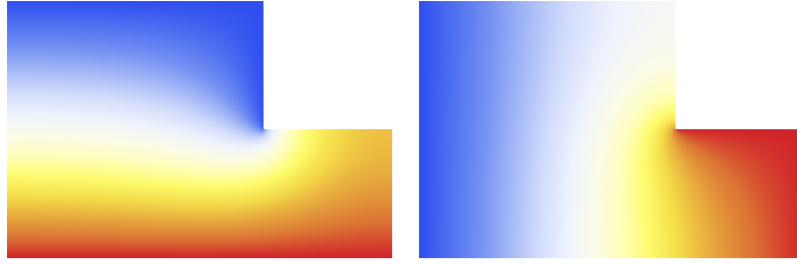


FIGURE 7. Potential functions in the case of L-shaped region 6.4. The vertices of the region Q are $z_1 = (0, 0)$, $z_2 = (3, 0)$, $z_3 = (3, 1)$, $z_4 = (2, 1)$, $z_5 = (2, 2)$ and $z_6 = (0, 2)$. Potential functions related to $M(Q; z_2, z_4, z_6, z_1) \approx 1.5081540958548603$ (left), and $M(Q; z_1, z_2, z_4, z_6) \approx 0.6630622181450123$ (right), are illustrated.

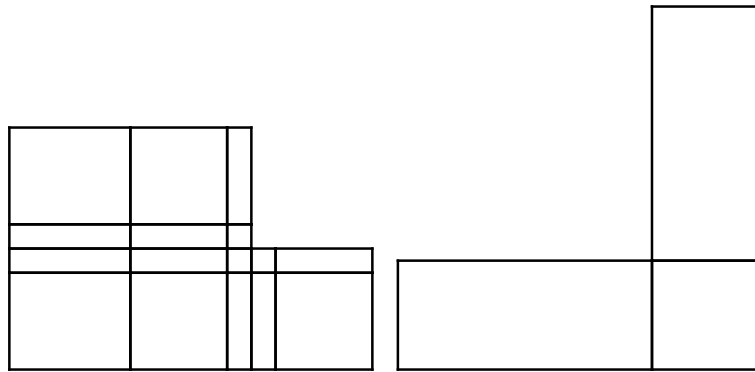


FIGURE 8. Minimal (see 3.16) meshes for domains of 6.4 and 7.1.

TABLE 2. Tests of (6.3) for L-shaped regions (see 6.4 and Figure 7), with (0.15, 12)-meshes used in the hp -method.

Method	Error range	
AFEM	$1.80 \cdot 10^{-10}$	$7.10 \cdot 10^{-10}$
SC Toolbox	$2.22 \cdot 10^{-16}$	$2.58 \cdot 10^{-14}$
hp -method ($p = 12$)	$4.01 \cdot 10^{-11}$	$1.59 \cdot 10^{-10}$
hp -method ($p = 16$)	$8.03 \cdot 10^{-13}$	$2.28 \cdot 10^{-12}$
hp -method ($p = 20$)	$5.98 \cdot 10^{-13}$	$1.80 \cdot 10^{-12}$

TABLE 3. Table for square in square, $p = 16$.

a	Capacity	Error (hp)	Error (SC)
0.1	2.83977741905223	$2.35 \cdot 10^{-15}$	$3.17 \cdot 10^{-14}$
0.2	4.134487024234081	$1.93 \cdot 10^{-15}$	$2.10 \cdot 10^{-15}$
0.3	5.632828000941654	$1.58 \cdot 10^{-16}$	$2.69 \cdot 10^{-16}$
0.4	7.5615315398105745	$1.17 \cdot 10^{-15}$	$1.50 \cdot 10^{-16}$
0.5	10.23409256936805	$1.74 \cdot 10^{-16}$	$3.42 \cdot 10^{-16}$
0.6	14.234879675824363	$7.49 \cdot 10^{-16}$	$1.35 \cdot 10^{-15}$
0.7	20.901581676413954	0.	$2.89 \cdot 10^{-16}$
0.8	34.23491519877346	$6.23 \cdot 10^{-16}$	$3.61 \cdot 10^{-16}$
0.9	74.23491519877882	$3.83 \cdot 10^{-16}$	$8.31 \cdot 10^{-15}$

TABLE 4. Table for cross in square, $p = 16$.

a	b	c	Capacity (SC)	Capacity (hp)	Difference
0.5	1.2	1.5	21.94721953515564	21.94721953515577	$5.99 \cdot 10^{-15}$
0.5	1.0	1.5	14.00279904484107	14.00279904484109	$8.88 \cdot 10^{-16}$
0.2	0.7	1.2	9.186926595881523	9.186926595881525	$1.93 \cdot 10^{-16}$
0.1	0.8	1.1	11.256582318490887	11.256582318490889	$1.58 \cdot 10^{-16}$
0.5	0.6	1.5	7.323269585560689	7.323269585567927	$9.88 \cdot 10^{-13}$
0.1	1.2	1.3	23.13861453810508	23.13861453810529	$8.91 \cdot 10^{-15}$

7. RING DOMAINS

In this section, we compare hp -FEM with exact values and with AFEM and SC Toolbox in certain ring domains. The square in square and cross in square cases were previously considered in [9] and numerical values were reported in [9, Table1, Table 4]. Our numerical results in Tables 3 and 4 provide 12 decimal places whereas in [9] only 6 decimal places were given.

7.1. Square in square. We compute here the capacity of the ring domain with plates $E = [-a, a] \times [-a, a]$ and $F = \mathbb{C}_\infty \setminus ((-1, 1) \times (-1, 1))$, $0 < a < 1$. The results with SC and the hp -method with (0.15, 16)-meshes are summarized in Table 1. For computation of the capacity, the ring domain is first split into four similar quadrilaterals. For the potential function, see Figure 10. Note that in this case, the exact values of the potential are known, see (4.14) and the related trapezoid type

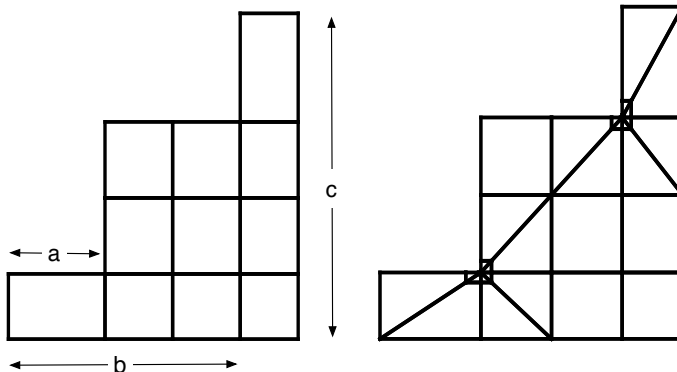


FIGURE 9. Meshing setup for cross in square.

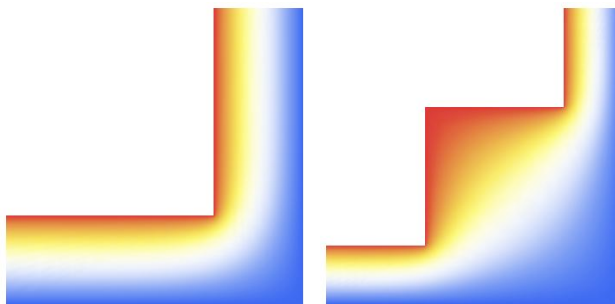


FIGURE 10. Potential functions: square in square and cross in square. Because of the symmetry, only one fourth of the picture is shown.

quadrilateral example. Explicitly, with $c = (1 - a)/(1 + a)$ and

$$u = \mu_{1/2}^{-1} \left(\frac{\pi c}{2} \right), \quad v = \mu_{1/2}^{-1} \left(\frac{\pi}{2c} \right), \quad r = \left(\frac{u - v}{u + v} \right)^2,$$

the capacity equals $4\pi/\mu_{1/2}(r)$.

7.2. Cross in square. Let $G_{ab} = \{(x, y) : |x| \leq a, |y| \leq b\} \cup \{(x, y) : |x| \leq b, |y| \leq a\}$. and $G_c = \{(x, y) : |x| < c, |y| < c\}$, where $a < c$ and $b < c$. We compute the capacity of the ring domain $R = G_c \setminus G_{ab}$. The results with SC and the hp -method with (0.15, 16)-meshes are summarized in Table 4. For computation of the capacity, the ring domain is again first split into four similar quadrilaterals. The mesh for the quadrilaterals is given in Figure 9, and the potential function is given in Figure 10. The exact values are not known in this case.

Since the underlying mesh topology remains constant in both examples above we have computed the results using exactly the same mesh template for every sub-problem, e.g. Figure 9 for Cross in square, $a = 0.5, b = 1.2, c = 1.5$, except for the extremal cases in terms of element distortion $a = 0.9$ for the square in square, and the case $a = 0.5, b = 0.6, c = 1.5$ for cross in square. Thus, the results also measure the robustness of the method with respect to moderate element distortion. Also, in

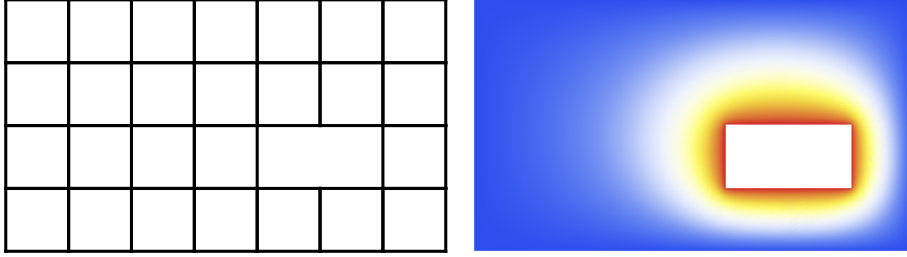


FIGURE 11. Rectangle in rectangle; $\{a, b, c, d\} = \{4, 1, 6, 2\}$, the minimal mesh and the potential function.

both cases due to symmetry we have graded the mesh only to the reentrant corners of the domain.

7.3. Rectangle in rectangle. Let $G_{abcd} = \{(x, y) : a \leq x \leq c, b \leq y \leq d\}$ and $G = \{(x, y) : 1 \leq x \leq 7, 1 \leq y \leq 4\}$. We compute the capacity of the ring domain $R = G \setminus G_{abcd}$. Here we consider a subset of possible cases when $a, b, c, d \in \mathbb{N}$. The results computed using the hp -method with $(0.15, 16)$ -meshes are summarized in Table 5. The potential function for the case $\{a, b, c, d\} = \{4, 1, 6, 2\}$ is given in Figure 11. The exact values are not known in this case.

Again, we have employed the same mesh template (simple quadrilateral grid as in Figure 9) over the entire test set. Grading has been used in the corners of G_{abcd} only. From results of Table 5 we can also see that some of the configurations are symmetric in terms of capacity. In these cases the differences in the computed values is less than 10^{-13} .

TABLE 5. Table for rectangle in rectangle.

a	b	c	d	p	Capacity
1	1	2	2	20	5.210320385649294
1	1	3	2	19	6.746053277945276
1	1	4	2	20	8.27007839293125
1	1	5	2	19	9.86240917550835
1	1	6	2	17	11.89718127369752
2	1	3	2	18	4.692072335693745
2	1	4	2	18	6.232078709256309
2	1	5	2	20	7.827105378062926
2	1	6	2	17	9.86240917550835
3	1	4	2	17	4.621123827863167
3	1	5	2	20	6.232078709256313
3	1	6	2	18	8.2700783929313
4	1	5	2	19	4.69207233569376
4	1	6	2	20	6.746053277945233
5	1	6	2	20	5.210320385649318

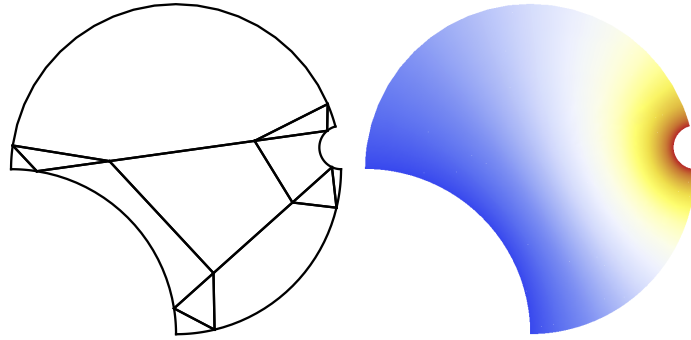


FIGURE 12. The quadrilateral $(Q_A; \pi/12, \pi, 3\pi/2, 1)$, the (final) mesh and the potential function. The relative error is $1.23 \cdot 10^{-13}$.

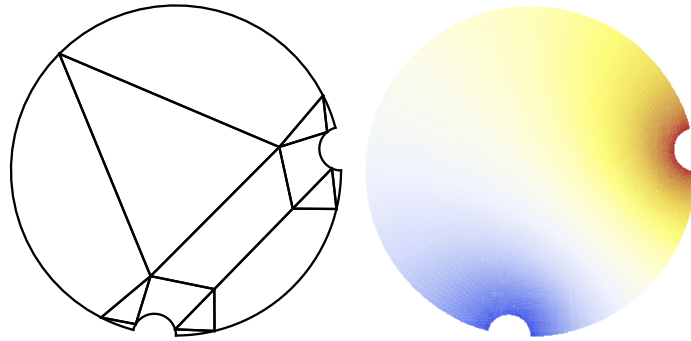


FIGURE 13. The quadrilateral $(Q_A; \pi/12, 17\pi/12, 3\pi/2, 1)$, the (final) mesh and the potential function. The relative error is $6.14 \cdot 10^{-14}$.

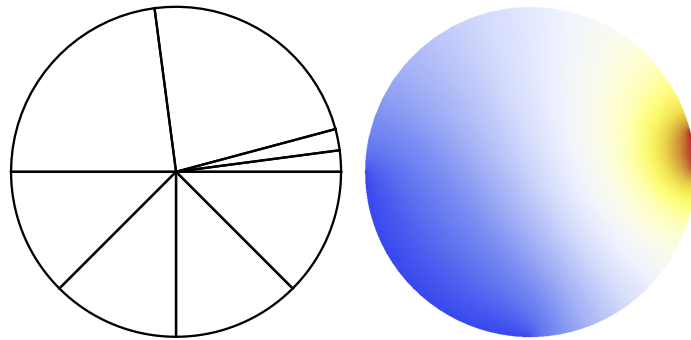


FIGURE 14. The quadrilateral $(Q_B; \pi/12, \pi, 3\pi/2, 1)$, the minimal mesh and the potential function. The relative error is $3.38 \cdot 10^{-11}$.

8. DOMAINS WITH CURVED BOUNDARIES

In this section, we give further examples featuring domains with curved boundaries. Simple examples of such domains are domains, where four or more points are connected with circular arcs. Some examples related to numerical methods and Schwarz-Christoffel formula for such domains can be found in the literature, e.g. [11].

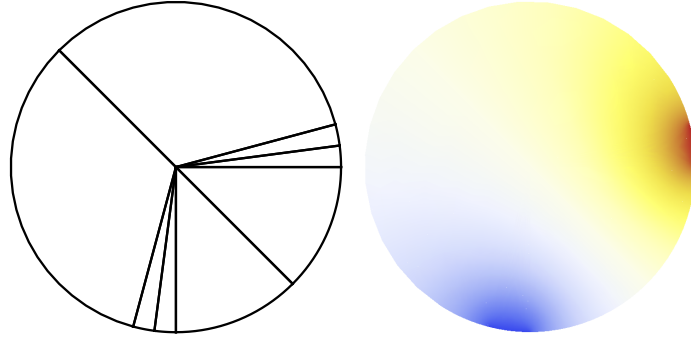


FIGURE 15. The quadrilateral $(Q_B; \pi/12, 17\pi/12, 3\pi/2, 1)$, the minimal mesh and the potential function. The relative error is $5.17 \cdot 10^{-11}$.

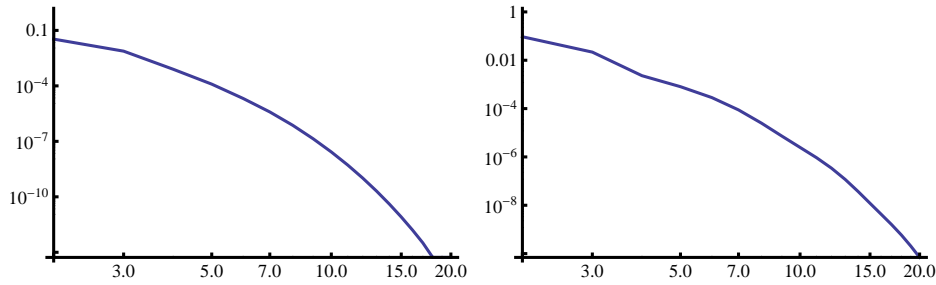


FIGURE 16. The p -convergence of the reciprocal error for the quadrilaterals $(Q_A; \pi/12, 17\pi/12, 3\pi/2, 1)$ (left) and $(Q_B; \pi/12, 17\pi/12, 3\pi/2, 1)$ (right). Logarithmic scale.

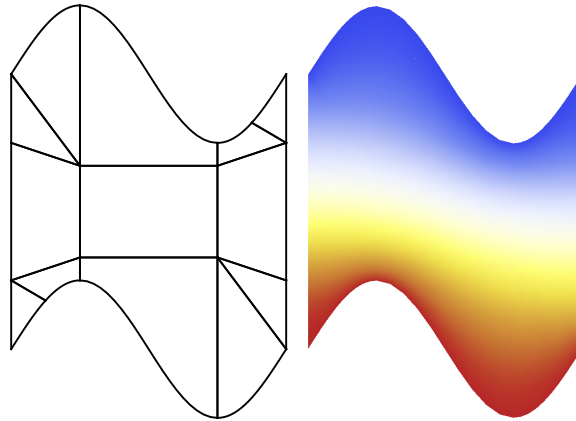


FIGURE 17. Wave: the minimal mesh and the potential function for 8.10.

Our method has the advantage that even more general quadrilaterals can be considered, as illustrated by examples given below. Here the meshing has been tuned by monitoring the rate of convergence in the polynomial degree. Both the minimal mesh and the scaling factor have been adjusted until exponential convergence in p has been observed. Two examples of exponential convergence, as predicted by Theorem 3.15, are shown in Figure 16.

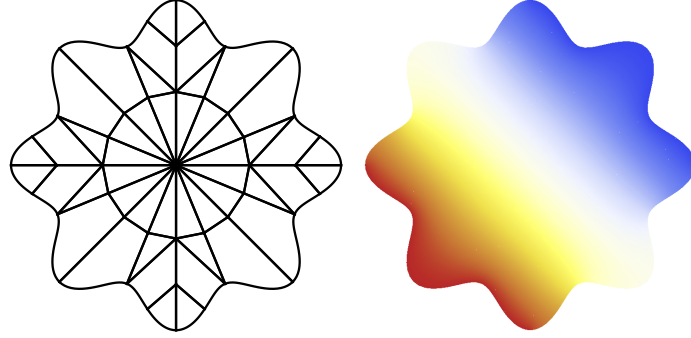


FIGURE 18. Flower I: the minimal mesh and the potential function. See also 8.11 and Table 8.

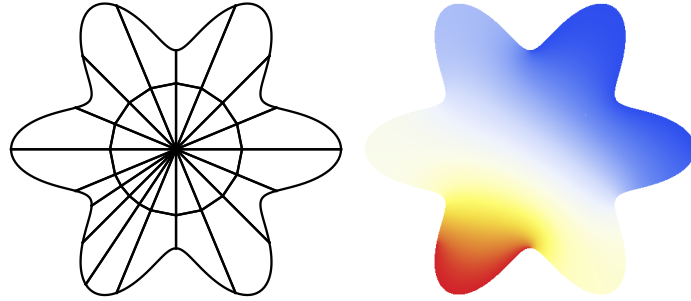


FIGURE 19. Flower II: the minimal mesh and the potential function. See also 8.11 and Table 9.

8.1. Circular quadrilaterals. The absolute ratio of four points $a, b, c, d \in \mathbb{C}$ is defined as

$$(8.2) \quad |a, b, c, d| = \frac{|a - c||b - d|}{|a - b||c - d|}.$$

The main property of the absolute ratio is the Möbius invariance:

$$(8.3) \quad |a, b, c, d| = |w(a), w(b), w(c), w(d)|,$$

if w is a Möbius transformation

$$(8.4) \quad w(z) = \frac{kz + l}{mz + n}, \quad (kn - ml \neq 0).$$

Given z_1, z_2, z_3 on a circle (or on a line) and w_1, w_2, w_3 on a circle (or on a line), there exists a Möbius transformation w with $w(z_j) = w_j$, $j = 1, 2, 3$.

8.5. Type A. Let us first consider a quadrilateral whose sides are circular arcs of intersecting orthogonal circles, i.e., angles are $\pi/2$. Let $0 < a < b < c < 2\pi$ and choose the points $\{1, e^a, e^b, e^c\}$ on the unit circle with the absolute ratio

$$(8.6) \quad |1, e^a, e^b, e^c| = \frac{\sin(b/2) \sin((c-a)/2)}{\sin(a/2) \sin((c-b)/2)} = u.$$

Let Q_A stand for the domain which is obtained from the unit disk by cutting away regions bounded by the two orthogonal arcs with endpoints $\{1, e^{ia}\}$ and $\{e^{ib}, e^{ic}\}$,

respectively. Then Q_A determines a quadrilateral $(Q_A; e^a, e^b, e^c, 1)$. Using a suitable Möbius transformation and the invariance (8.3) we can map Q_A onto the upper half of the annulus $\{z \in \mathbb{C} : 1 < |z| < t\}$ and we obtain the following formula:

$$(8.7) \quad \mathbf{M}(Q_A; e^a, e^b, e^c, 1) = \pi / \log t,$$

i.e. a half of the modulus of the full annulus, where

$$t = 2u - 1 + 2\sqrt{u^2 - u}, \quad t > 1.$$

The results are summarized in Table 6.

TABLE 6. Moduli of quadrilaterals $(Q_A; e^{im\pi/24}, e^{in\pi/24}, e^{ir\pi/24}, 1)$ for several integer triples (m, n, r) computed with the hp -method, $p = 20$.

Nodes	Reference	Computed value	Relat. error	Recipr. error
(2, 10, 12)	0.7071508111121534	0.7071508111121347	$2.64 \cdot 10^{-14}$	$1.02 \cdot 10^{-13}$
(2, 10, 14)	0.8074514311467651	0.8074514311467831	$2.23 \cdot 10^{-14}$	$2.55 \cdot 10^{-14}$
(4, 12, 18)	1.0383251171675787	1.0383251171675796	$8.55 \cdot 10^{-16}$	$1.44 \cdot 10^{-15}$
(6, 16, 24)	1.170060906774661	1.1700609067746603	$5.69 \cdot 10^{-16}$	$2.22 \cdot 10^{-15}$
(8, 22, 32)	1.313262425617007	1.3132624256170076	$5.07 \cdot 10^{-16}$	$3.33 \cdot 10^{-16}$

8.8. Type B. Next we let the sides of the quadrilateral be circular arcs be of the unit disk, and in this case all the angles are equal to π . Now the unit disk, together with the boundary points $e^a, e^b, e^c, 1$ determines a quadrilateral which we denote by Q_B . Using an auxiliary Möbius transformation of the unit disk onto the upper half plane we can readily express the modulus using the capacity of the Teichmüller ring domain [4, Section 7] and express it as follows

$$(8.9) \quad \mathbf{M}(Q_B; e^a, e^b, e^c, 1) = \frac{1}{2}\tau(u - 1),$$

where u is as in (8.6), and

$$\tau(t) = \pi / \mu_{1/2}(1/\sqrt{1+t}), \quad t > 0,$$

and $\mu_{1/2}(r)$ is as in (4.9), gives the conformal capacity of the plane Teichmüller ring. The results are summarized in Table 7.

TABLE 7. Moduli of quadrilaterals $(Q_B; e^{im\pi/24}, e^{in\pi/24}, e^{ir\pi/24}, 1)$ for several integer triples (m, n, r) computed with the hp -method, $p = 20$.

Nodes	Reference	Computed value	Relat. error	Recipr. error
(2, 10, 12)	0.5389714947317054	0.5389714947624924	$5.71 \cdot 10^{-11}$	$7.68 \cdot 10^{-11}$
(2, 10, 14)	0.5953434982171909	0.5953434982359955	$3.16 \cdot 10^{-11}$	$4.26 \cdot 10^{-11}$
(4, 12, 18)	0.7121629047455362	0.7121629047457778	$3.39 \cdot 10^{-13}$	$6.06 \cdot 10^{-13}$
(6, 16, 24)	0.7718690862645192	0.7718690862646902	$2.22 \cdot 10^{-13}$	$4.09 \cdot 10^{-13}$
(8, 22, 32)	0.8319009599091923	0.8319009599093506	$1.90 \cdot 10^{-13}$	$3.48 \cdot 10^{-13}$

Next we consider non-convex examples featuring quadrilaterals with curved boundaries which are not circular segments.

8.10. Wave. Let $Q = \{(x, y) : 0 < x < 1, \sin(2\pi x)/4 < y < 1 + \sin(2\pi x)/4\}$, and $z_1 = (0, 0)$, $z_2 = (1, 0)$, $z_3 = (1, 1)$, $z_4 = (0, 1)$. Then the hp -method with $p = 20$ gives $M(Q; z_2, z_3, z_4, z_1) \approx 1.285385932609546$. An error estimate based on the reciprocal identity (4.1) is $2.66 \cdot 10^{-15}$. For visualization, see Figure 17.

8.11. Flowers. Let Q be the domain bounded by the curve $r(\theta) = 0.8 + t \cos(n\pi\theta)$, $0 \leq \theta \leq 2\pi$, $n = 4, 6, 8$ and $t = 0.1$ or $t = 0.2$. Domains of this type are illustrated in Figures 18 and 19. We compute moduli of quadrilaterals $M(Q; z_1, z_2, z_3, z_4)$, where $z_j = r(\theta_j)$. We consider flower shaped quadrilaterals of type I with $\theta_j = (j - 1)\pi/2$ for $j = 1, 2, 3, 4$, and type II, where $\theta_1, \theta_2, \theta_3$ are as before, and $\theta_4 = 5\pi/4$ (see Figures 18 and 19). The numerical results are summarized in Tables 8 and 9.

TABLE 8. Moduli of flower-shaped quadrilaterals (t, n) of type I computed with the hp -method, $p = 20$. Note that, because of symmetry, it follows from (4.1) that the exact value of modulus is 1.

n	Error ($t = 0.1$)	Error ($t = 0.2$)
4	$3.18 \cdot 10^{-14}$	$2.25 \cdot 10^{-14}$
6	$3.74 \cdot 10^{-11}$	$8.45 \cdot 10^{-11}$
8	$1.34 \cdot 10^{-13}$	$6.27 \cdot 10^{-11}$

TABLE 9. Moduli of flower-shaped quadrilaterals (t, n) of type II computed with the hp -method, $p = 20$. The error estimate is obtained by using the reciprocal identity (4.1).

n	t	Error	Modulus
4	0.1	$2.00 \cdot 10^{-15}$	0.8196442147286799
4	0.2	$1.40 \cdot 10^{-13}$	0.8196441884805612
6	0.1	$2.34 \cdot 10^{-14}$	0.7896695654987764
6	0.2	$1.43 \cdot 10^{-10}$	0.7690460663235661
8	0.1	$9.05 \cdot 10^{-14}$	0.8196441884804566
8	0.2	$1.38 \cdot 10^{-10}$	0.8196441885295815

9. SUMMARY

The computation of the moduli of quadrilaterals and ring domains with piecewise smooth boundaries is a problem frequently occurring in various applications, see [34]. There is no general method for such computations except perhaps the case of polygonal quadrilaterals when the SC Toolbox [17, 18] may be considered as the “state-of-the-art” tool. For the case of ring domains there is no such general tool, but the adaptive finite element software AFEM of K. Samuelsson [9] has turned out to be effective in a number of cases reported in [9]. For the purposes of this paper the so called hp -FEM method implemented by H. Hakula, and first reported in this paper, is used in several examples with curvilinear boundaries where the previous methods do not apply. The hp -FEM method, applied to the computation of moduli of two

ring domains previously considered in [9] and reported in Tables 3 and 4, provide a significant improvement over the values reported in [9].

For experimental error estimate we have used so called reciprocal identity, which we have not seen used anywhere for the purpose of error estimation. It is our belief that this simple identity should be more widely known. It provides a criterion for estimating the error of numerical computation of the modulus of a quadrilateral for a very large class of simply connected domains, including those with curved boundaries. It seems that such a large class of examples has previously not been known for instance in the FEM community. These examples also enable one to experimentally demonstrate the theoretical convergence rates in nontrivial model problem cases as we have shown for the case of hp -FEM.

For the very special case of convex polygons with four sides, the modulus of the corresponding quadrilateral is known as an analytic-numeric formula (4.11) by [22] and this is our starting point. We compare the performance of SC Toolbox, AFEM, and hp -FEM against the formula [22] and the reciprocal identity test. Next, again using SC Toolbox, AFEM, and hp -FEM, we consider polygonal quadrilaterals with more sides, L-shaped quadrilaterals and carry out similar comparison, using again the reciprocal identity as the test quantity. Thereafter, we discuss, now using AFEM, and hp -FEM, two classical cases of ring domains, the square frame and the cross in square ring domains previously considered e.g. in [9] where further references may be found. The error estimate in the square frame case is based on the well-known formula (4.14) whereas for the cross in square case we use SC Toolbox and the results from [9] as the comparison data. Finally, we also consider several cases of quadrilaterals with curvilinear boundaries, now only using the hp -FEM method, because the other methods mentioned above do not apply.

Acknowledgments. We are indebted to the referees for very valuable sets of suggestions concerning the presentation of the results and the use of the SC Toolbox. We also thank Prof. N. Papamichael for his helpful comments on this paper.

REFERENCES

- [1] L.V. AHLFORS, *Conformal invariants: topics in geometric function theory*. McGraw-Hill Book Co., 1973.
- [2] K. AMANO, *A charge simulation method for numerical conformal mapping onto circular and radial slit domains*, SIAM J. Sci. Comput. 19 (1998), no. 4, 1169–1187.
- [3] G.D. ANDERSON, S.-L. QIU, M.K. VAMANAMURTHY and M. VUORINEN, *Generalized elliptic integrals and modular equations*, Pacific J. Math. 192 No. 1 (2000), 1–37.
- [4] G.D. ANDERSON, M.K. VAMANAMURTHY and M. VUORINEN, *Conformal invariants, inequalities and quasiconformal mappings*, Wiley-Interscience, 1997.
- [5] I. BABUŠKA and B. GUO, *Regularity of the solutions of elliptic problems with piecewise analytical data, parts I and II*, SIAM J. Math. Anal., 19, (1988), 172–203 and 20, (1989), 763–781.
- [6] I. BABUŠKA and B. GUO, *Approximation properties of the hp -version of the finite element method*, Comp. Meth. Appl. Mech. Engr., 133, (1996), 319–346.
- [7] I. BABUŠKA and M. SURI, *The P and H - P versions of the finite element method, basic principles and properties*, SIAM Review 36 (1994), 578–632.
- [8] L. BANJAI, *Revisiting the crowding phenomenon in Schwarz-Christoffel mapping*. SIAM J. Sci. Comput. 30 (2008), no. 2, 618–636.

- [9] D. BETSAKOS, K. SAMUELSSON and M. VUORINEN, *The computation of capacity of planar condensers*, Publ. Inst. Math. 75 (89) (2004), 233–252.
- [10] F. BOWMAN, *Introduction to Elliptic Functions with applications*, English Universities Press Ltd., London, 1953.
- [11] P.R. BROWN, *Mapping onto circular arc polygons*, Complex Variables, Theory Appl. 50 (2005), No. 2, 131–154.
- [12] W. BURNSIDE, *Problem of Conformal Representation*, Proc. London Math. Soc. (1) 24 (1893), 187–206.
- [13] D. CROWDY, *Geometric function theory: a modern view of a classical subject*, Nonlinearity 21 (2008), no. 10, T205–T219.
- [14] D. CROWDY and J. MARSHALL, *Constructing multiply connected quadrature domains*, SIAM J. Appl. Math. 64 (2004), no. 4, 1334–1359.
- [15] T.K. DELILLO, T.A. DRISCOLL, A.R. ELCRAT and J.A. PFALTZGRAFF, *Radial and circular slit maps of unbounded multiply connected circle domains*, Proc. R. Soc. Lond. Ser. A Math. Phys. Eng. Sci. 464 (2008), no. 2095, 1719–1737.
- [16] L. DEMKOWICZ, *Computing with hp-Adaptive Finite Elements, Vol. 1*, Chapman & Hall/CRC, 2006.
- [17] T.A. DRISCOLL, *Schwarz-Christoffel toolbox for MATLAB*, <http://www.math.udel.edu/~driscoll/SC/>
- [18] T.A. DRISCOLL and L.N. TREFETHEN, *Schwarz-Christoffel mapping*. Cambridge Monographs on Applied and Computational Mathematics, 8. Cambridge University Press, Cambridge, 2002.
- [19] V. DUBININ and M. VUORINEN, *On conformal moduli of polygonal quadrilaterals*. Israel J. Math 171 (2009), 111–125, DOI:10.1007/s11856-009-0043-8, arXiv math.CV/0701387
- [20] D. GAIER, *Conformal modules and their computation*, in ‘Computational Methods and Function Theory’ (CMFT’94), R.M.Ali *et al.* eds., 159–171. World Scientific, 1995.
- [21] W.J. GORDON and C.A. HALL, *Transfinite element methods: blending function interpolation over arbitrary curved element domains*, Numer. Math. 21 (1973), 109–129.
- [22] V. HEIKKALA, M.K. VAMANAMURTHY and M. VUORINEN, *Generalized elliptic integrals*, Comput. Methods Funct. Theory 9 (2009), 75–109. arXiv math.CA/0701436.
- [23] P. HENRICI, *Applied and Computational Complex Analysis, vol. III*, Wiley-Interscience, 1986.
- [24] C. HU, *A software package for computing Schwarz-Christoffel conformal transformation for doubly connected polygonal regions*, ACM Transactions of Math. Software 24 (1998).
- [25] N. HYVÖNEN, *Complete electrode model of electrical impedance tomography: Approximation properties and characterization of inclusions*, SIAM J. Appl. Math. 64 (2004), 902–931.
- [26] R. KÜHNAU, ED.: *Handbook of complex analysis: geometric function theory*. Vol. 1-2. North-Holland, Amsterdam, 2002 and 2005.
- [27] R. KÜHNAU, *The conformal module of quadrilaterals and of rings*, In: *Handbook of Complex Analysis: Geometric Function Theory*, (ed. by R. Kühnau) Vol. 2, North Holland/Elsevier, Amsterdam, 99–129, 2005.
- [28] P.K. KYTHE, *Computational conformal mapping*, Birkhäuser, 1998.
- [29] O. LEHTO and K.I. VIRTANEN, *Quasiconformal mappings in the plane*, 2nd edition, Springer, Berlin, 1973.
- [30] X.-J. LUO, M.S. SHEPHARD, J.-F. REMACLE, R.M. O’BARA, M.W. BEALL, B. SZABO, and R. ACTIS, *p-Version Mesh Generation Issues*, IMR 2002, 343–354.
- [31] D.E. MARSHALL and S. ROHDE, *Convergence of a variant of the zipper algorithm for conformal mapping*, SIAM J. Numer. Anal. 45 (2007), no. 6, 2577–2609.
- [32] N. PAPAMICHAEL, *Dieter Gaier’s contributions to numerical conformal mapping*, Comput. Methods Funct. Theory 3 (2003), no. 1–2, 1–53.

- [33] N. PAPAMICHAEL and N.S. STYLIANOPOULOS, *The asymptotic behavior of conformal modules of quadrilaterals with applications to the estimation of resistance values*, Constr. Approx. 15 (1999), no. 1, 109–134.
- [34] N. PAPAMICHAEL and N.S. STYLIANOPOULOS, *Numerical Conformal Mapping: Domain Decomposition and the Mapping of Quadrilaterals*, World Scientific, 2010.
- [35] R.M. PORTER, *An interpolating polynomial method for numerical conformal mapping*. SIAM J. Sci. Comput. 23 (2001), no. 3, 1027–1041.
- [36] R.M. PORTER, *History and Recent Developments in Techniques for Numerical Conformal Mapping*, Proceedings of the International Workshop on Quasiconformal Mappings and Their Applications (IWQCMA05), Dec 27, 2005 – Jan 1, 2006, IIT Madras, edited by S. Ponnusamy, T. Sugawa, M. Vuorinen, (2007), 207–238, Narosa Publ Co, ISBN 81-7319-807-1.
- [37] R. SCHINZINGER and P. LAURA, *Conformal Mapping: Methods and Applications*, Elsevier, Amsterdam 1991.
- [38] CH. SCHWAB, *p- and hp-Finite Element Methods*, Oxford University Press, 1998.
- [39] E. SHARON and D. MUMFORD, *2D-Shape analysis using conformal mapping*, Intern. J. Computer Vision 70(1), 2006, DOI:10.1007/s11263-006-6121-z
- [40] B. SZABO and I. BABUŠKA, *Finite Element Analysis*, Wiley, 1991.
- [41] L.N. TREFETHEN, *Numerical computation of the Schwarz-Christoffel transformation*. SIAM J. Sci. Statist. Comput. 1 (1980), no. 1, 82–102.
- [42] L.N. TREFETHEN and T.A. DRISCOLL, *Schwarz-Christoffel mapping in the computer era*. Proceedings of the International Congress of Mathematicians, Vol. III (Berlin, 1998). Doc. Math. 1998, Extra Vol. III, 533–542.
- [43] R. WEGMANN, *Methods for numerical conformal mapping*, Handbook of complex analysis: geometric function theory. Vol. 2, (ed. by R. Kühnau), Elsevier, Amsterdam, 351–477, 2005.

E-mail address: harri.hakula@tkk.fi

AALTO UNIVERSITY, INSTITUTE OF MATHEMATICS, P.O. BOX 11100, FI-00076 AALTO, FINLAND

E-mail address: antti.rasila@iki.fi

AALTO UNIVERSITY, INSTITUTE OF MATHEMATICS, P.O. BOX 11100, FI-00076 AALTO, FINLAND

E-mail address: vuorinen@utu.fi

DEPARTMENT OF MATHEMATICS, FI-20014 UNIVERSITY OF TURKU, FINLAND